Control of translational and rotational movement at nanoscale

Štacko, Peter

Chapter V:

Tidal locking of aromatic moieties in a molecular motor

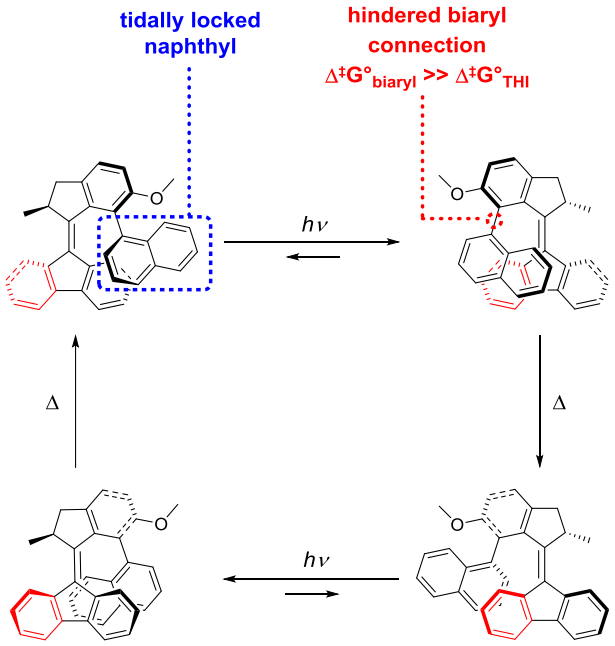

A molecular motor with an intrinsic biaryl moiety has been conceived and demonstrated to exhibit a movement of the biaryl coupled to the photochemically driven, unidirectional rotary movement of the molecular motor. The naphthyl moiety of the biaryl unit slides along the lower half in a geared manner during photochemical E-Z isomerization, followed by a geared rotation around the lower half while undergoing the thermal helix inversion, thus retaining the configuration of the biaryl after every cycle of the motor. The system therefore displays tidal-locking behavior of the naphthyl moiety with respect to the molecular motor.

Štacko, P.; Kistemaker, J. C. M.; van Leeuwen, T.; Chang, M. C.; Otten, E.; Feringa, B. L. *Science*, **2017**, *356*, 6341, 964-968

Introduction

Controlling both rotational and translational molecular motion and achieving further translation and propagation of the motion as well as exploring dynamic functions, taking inspiration from Nature's nanomachines, still remains a considerable challenge in today's chemistry.[1-3] Artificial molecular motors have been shown to enable movement at nanoscale[4-9], as well as achieve dynamic control of mechanical, electronic and transport properties.[10-20] The inherent benefits of artificial molecular devices and motors that simulate aspects of complex biological systems might include simpler design, ease of control under various conditions which are not limited to biologically compatible environments and control of a wide variety of dynamic functions. In many cases, such molecular devices are based on photoswitchable units thereby facilitating precise control using light as a non-invasive stimulus with excellent spatio-temporal resolution. Recently, several application of nanosystems based on switches and motors have emerged, including systems for molecular electronics[21,22], logics [23,24], delivery [15,25-28], adaptive materials[29-31] and responsive surfaces[27,32], and switchable catalysts[33-35]. ATPase-mediated transport[36], flagella-based bacterial movement[37] and protein translocation performed by living organisms are a few examples demonstrating that directionality of motion is of fundamental importance for the function of biological nanoscale machines. Simultaneously, amplification, propagation and coupling of the movement to other components as seen in, for instance, geared wheels and sprockets in the macroscopic world, continue to be largely unexplored, yet highly desirable.

The area of geared rotation has been pioneered in the '70s and '80s mostly by Mislow starting with the rotation of alkyl groups around single carbon-carbon bond in alkanes, substituted benzenes and triptycenes.[38-41] More elaborate system of triptycenes linked with a short tether that act as a pair of almost frictionless bevel gears was introduced where the disrotatory cogwheeling motion arises from complementary steric interactions between tightly fitting rotors (Figure 1).[42-44] Several other systems based on this concept have been synthesized to this date[45-47], including desymmetrized spur gear molecule with bibenzimidazole-based stator.[48] While exhibiting geared movement, neither of the systems mentioned hitherto display unidirectional behavior since probability of rotation in either direction is equal as no chirality or other source of bias is introduced.

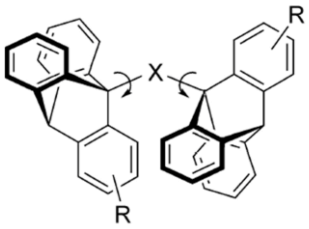

Figure 1. Two tethered triptycenes acting as a pair of bevel gears.

Taking advantage of light-driven rotary motors our group, has previously shown that a rate of rotation of an aryl rotor can be adjusted by alteration of conformation of the adjacent molecular motor, manifesting a coupled state of the two parts.[49] Other systems featuring geared rotation around single carbon-carbon include the rotation of alkyl groups in highly crowded alkanes[50,51] as well as tertiary aromatic amides as reported by Clayden.[52,53] In this case, it was shown that while the barrier to gear slippage is low, at least 90% of the rotations about the Ar—CO bond are synchronous with the rotation about the C—N bond in the amides. In a somewhat advanced design, Carella *et al*. proposed that the phenyls of the ligand in a ruthenium sandwich complex are forced to twist out of their perpendicular arrangement to allow the indazolyl rings to pass, corresponding to a coupled rotation mechanism (Figure 2).

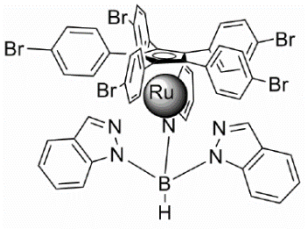

Figure 2. Ruthenium sandwich-type complex exhibiting a geared rotation mechanism.

Another example of a sandwich complex demonstrates transmission of rotational activities through mechanical interactions between two rotors attached to a lanthanum porphyrin double-decker (Figure 3).[54] The geared behavior could be toggled off and on by addition of triethylamine and trifluoroacetic acid, respectively, by modulation of the interaction between the two porphyrin units upon (de-)protonation.

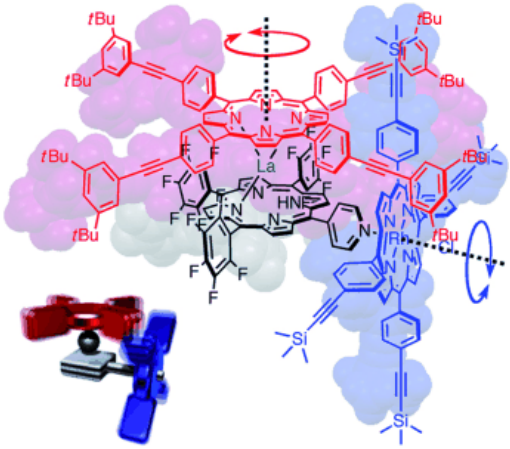

Figure 3. Lanthanum sandwich complex with the appending two rotors operating in a geared fashion and the schematic representation of the device. (Reproduced from ref. 54)

Employing porphyrins, the group Anderson demonstrated a formation of caterpillar track complexes in which two template wheels bind inside a nanoring (Figure 4a).[55] NMR exchange spectroscopy (EXSY) experiments revealed that the complexes exhibit correlated motion, in which the conrotatory (unlike in a gear where it is disrotatory) rotation of the two template wheels is coupled to rotation of the nanoring track (Figure 4b). In addition, addition of $PdCl_2$ and thus complexation of the two wheels prevented the caterpillar track motion.

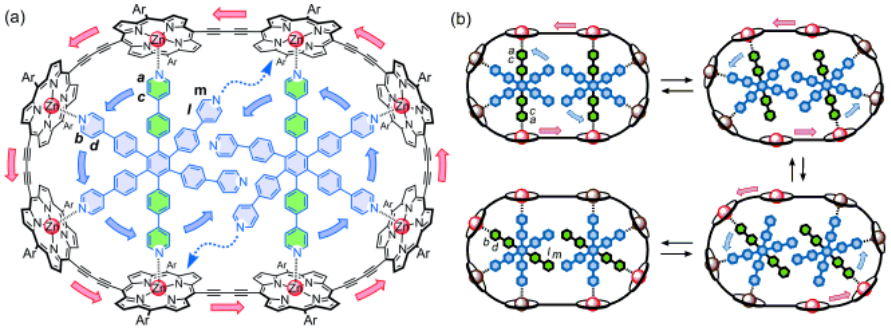

Figure 4. (a) Detailed molecular structure of the caterpillar track complex. (b) Mechanism leading to a concerted 60° rotation of both template units, transforming environments *a* and *c* into *b*/*m* and *d*/*l*. According to this mechanism, both template units must rotate in the same direction, but the direction of rotation is arbitrary, and subsequent steps could occur in either direction with equal probability. (Reproduced from ref. 55)

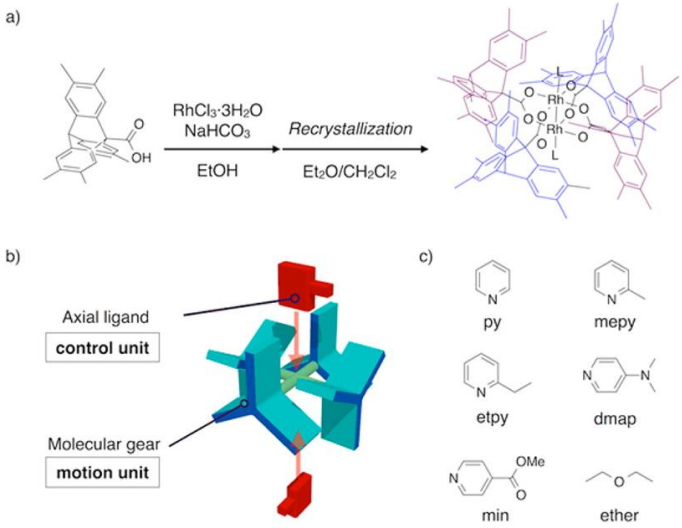

Figure 5. (a) Synthesis and chemical structure of the dirhodium-centered four-gear complex. (b) Schematic representation of rotational control by the axial ligand exchange. (c) Axial ligands used in the study. (Reproduced from ref. 57)

Geared behavior has also been observed in other organometallic compounds such as platinum(II) complex[56] or a dirhodium-centered complex chelated with four triptycene carboxylates and two axial ligands[57] (Figure 5). The latter system constitutes an example where a dynamic control over rates of rotation in solution can be achieved by exchange of axial ligands. The rate of rotation was

found to correlate with the coordination ability and the bulkiness of the ligands as well as changes in the electronic states of the dirhodium center.

The group of Kira demonstrated the possibility to implement a clutch into these types of systems and conceived a silane-bridged triptycene system (Scheme 1).[58] Exploiting high affinity of silicon towards fluoride, the system could be chemically declutched-clutched in a reversible fashion by addition of KF/18-Crown-6 and H_2O, respectively. Nucleophilic attack of fluoride on the silicon atom leads to a change of hybridization of Si from sp^3 do sp^3d, thus forcing different relative orientation of the two appending triptycyls and relief of the steric repulsion between them.

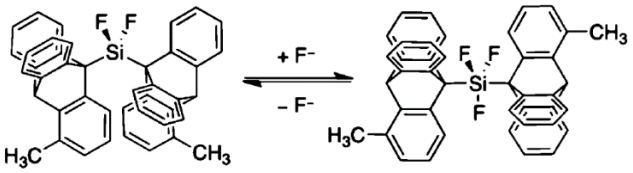

Scheme 1. The mechanism of declutching-clutching in the silane-bridged triptycene developed by group of Kira. (Reproduced from ref. 58)

Design of the system

The structure of a typical second generation molecular motor comprises an upper and lower half connected by a central olefinic bond, which serves as the axle of rotation.[59] The combination of helical structure, stereogenic center, stilbene type photoisomerization and thermal helix inversion allows unidirectional light-driven rotary motion. We envisioned that introducing an aryl substituent (R=Ar) (Figure 6) in the fjord region of such a molecular motor would result in a controlled biaryl motion governed by the photochemically induced unidirectional rotation of the overcrowded alkene. The four-step rotary cycle and the sliding motion and conformational change of the aryl rotor are schematically depicted in Figure 6. During the 360 degree rotation of the motor one side of the aryl rotor continuously faces the lower half of the molecular motor akin to the *tidal locking* of the moon to the earth where only one side of the moon continuously faces the earth. To ensure such a synchronous rotation, random biaryl rotation (BR) has to be suppressed by providing a barrier for the biaryl rotation which is sufficiently higher than the barrier for the thermal helix inversion (THI) of the motor during its rotary process. Thus, such relative

barriers of the two competing thermal processes would fully prevent biaryl rotation throughout the photochemically driven rotary cycle of the molecular motor.

It was anticipated that the aryl moiety (indicated in red) would slide along the lower half of the motor (in black) in the course of the photochemical *E*-*Z* isomerization, adjusting the dihedral angle around the single bond of the biaryl, thus minimizing the steric repulsion between the aryl and the lower half in the metastable form of the molecular motor (step 1, Figure 6). A subsequent thermal helix inversion (step 2) proceeds unidirectionally due to the unfavorable pseudoequatorial orientation of the methyl group at the stereogenic center. In this step again, the dihedral angle around the biaryl single bond is adjusted but BR is prevented. Subsequent photochemical (step 3) and thermal (step 4) steps complete a 360° cycle. A considerably higher barrier for biaryl rotation than for helix inversion would ensure that the aryl rotates around the lower half in a synchronous manner, thereby keeping the same side of the aryl facing the lower half of the motor during the entire rotational cycle.

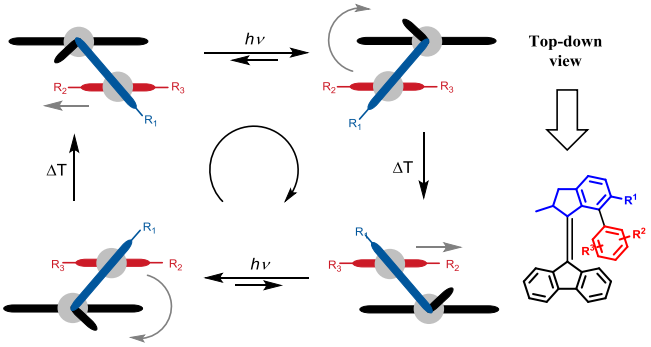

Figure 6. Schematic representation of the rotatary cycle of as viewed from the top along the axis given by the double bond. Upper half moiety (blue); fluorenyl lower half (black); naphthalene moiety (red).

To prove the tidal locking in such a molecular motor, three requirements have to be fullfilled: (i) retention of the absolute stereochemistry (R_a/S_a) over the biaryl bond during the photochemical *E*-*Z* isomerization (i.e. a single face of the aryl keeps facing the lower half), however, it is not excluded that the helicity of the biaryl chromophore (*P*/*M*) is inverted during the isomerization (*vide infra*, Figure 9); (ii) retention of the absolute stereochemistry over the biaryl bond during the thermal helix inversion; (iii) a temperature at which the thermal helix

inversion takes place at an appreciable rate while the rate of biaryl rotation is negligibly low. Three sites of modification (R^1, R^2 and R^3 in Figure 7) have been designated in order to achieve a 'tidally locked' biaryl on a molecular motor. A symmetric substitution pattern on the biaryl moiety (R_2 and R_3) such as bis-*meta*-phenylacetylene-benzene or 9-anthracene would provide an elegant system, with inherently identical barriers on both sides of the biaryl rotation axis. Quantifying the biaryl rotation barrier can simply be achieved by NMR coalescence experiment, however, it would not be possible to prove absence of biaryl rotation during PEZ or THI on account of the biaryl's symmetric nature. Therefore, asymmetry has to be introduced into the biaryl to allow for the existence of two distinguishable atropoisomers. This is easily accomplished by the removal of all substituents on one side (R^3) providing a moiety such as 1-naphthalene, however, this is expected to lower the barrier for biaryl rotation on the R^3 side, which in turn can be prevented by the use of a simple 'brake' moiety, as small as a methoxy group, at R^1. Thus, the molecular motor **1** was designed and proposed as a candidate for further theoretical and experimental investigation (Figure 7).

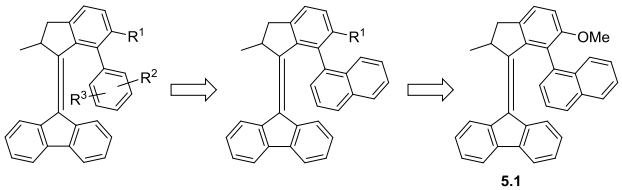

Figure 7. Progression of the design of a biaryl tidally-locked molecular motor.

The system described hitherto features three stereochemical elements. The stereogenic center of the motor can exist with both the *R* and *S* configuration. The second element is the helicity of the overcrowded alkene which is directly linked to the configuration at the allylic stereogenic center. For instance, in the *S* enantiomer of the motor, the diastereoisomer of lowest energy (the stable form) possesses the *M* helicity, while the higher energy diastereoisomer (the metastable form) possesses *P* helicity. The third stereochemical element is the axial chirality over the biaryl bond, of which the absolute stereoisomers, according to the CIP rules, are assigned R_a and S_a. For biphenyls with an average bite-angle of 90°, such as *ortho* substituted biphenyls, these stereochemistry descriptors are interchangeably used with *M* and *P*, respectively.[60] However, this becomes problematic when the bite-angle is smaller than 90°, which can be observed in hindered systems (*vide infra*) or non-*ortho* substituted biphenyls at

low temperature (e.g. unsubstituted biphenyl possesses a bite-angle of 44.4°).[61] In such examples, each stereoisomer with R_a and S_a absolute configuration possesses two conformational helical geometries, and when considering the helical procession of the two aromatic planes analogous to the alkene chromophore, these two conformations can be assigned as right-handed (*P*) or left-handed (*M*). Hence, four different conformations of the biphenyl are theoretically possible (Figure 8).

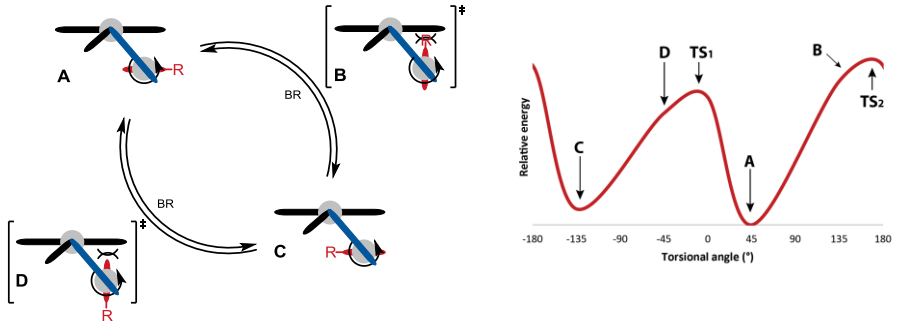

Figure 8. (left) Depiction of the four possible conformations of the biaryl moiety as viewed from the top along the central double bond. (right) Energy diagram showing the two conformers with the aryl perpendicular to the lower half (B and D) experience sterical hindrance.

In this specific system, practically, only the conformation in which the biaryl is parallel to the fluorenyl is expected, as the other conformation, with the biaryl orientated perpendicular with respect to the lower half, induces significant steric strain (Figure 8). With such a constraint, the true helicity (*P*/*M*) of the biaryl is inextricably connected to the helicity (*P*/*M*) of the overcrowded alkene chromophore, and will be identical to it in each isomer. Therefore, three stereodescriptors (*R*/*S*, *P*/*M* and R_a/S_a) will be sufficient for the description of any expected isomer in the coupled rotary cycles. However, at certain points we will make use of an additional stereodescriptor to provide extra clarification of the torsion angle of the biaryl moiety (*syn* (*s*) = 0°–±90°, *anti* (*a*) = ±90°–180°, *clinal* (*c*) = 30°–150°/−30°–−150°, *periplanar* (*p*) = −30°–30°/−150°–150°). The asterisks at the stereodescriptors throughout the text denote a racemic mixture with identical relative stereochemistry (S^*,M^*,S_a^* means a mixture of *S*,*M*,S_a and *R*,*P*,R_a).

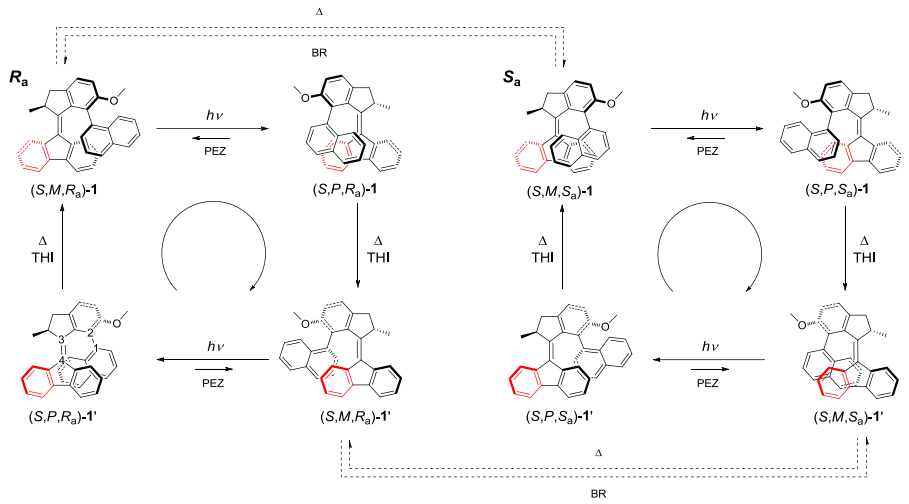

Figure 9. R_a: Rotational cycle of (*S*,*M*,R_a)-**1**. The naphthalene moiety slides along the fluorenyl lower half during the photochemical *E*-*Z* isomerisation (from stable (*S*,*M*,R_a)-**1** to metastable *(S,P,*R_a)-**1**), followed by rotating around the fluorenyl in a synchronous fashion during the thermal helix inversion (from metastable *(S,P,*R_a)-**1** to stable (*S*,*M*,R_a)-**1**). S_a: Rotational cycle of *(S,M,*S_a)-**1**. The naphthalene moiety slides along the fluorenyl lower half during the photochemical *E*-*Z* isomerisation (from stable *(S,M,*S_a)-**1** to metastable *(S,P,*S_a)-**1**), followed by rotating around the fluorenyl in a synchronous fashion during the thermal helix inversion (from metastable *(S,P,*S_a)-**1** to stable *(S,M,*S_a)-**1**); (PEZ, photochemical *E*-*Z* isomerization; THI, thermal helix inversion; BR, biaryl rotation). Note: $t_{1/2}$(BR) >> $t_{1/2}$(THI).

The anticipated rotational cycles for the two atropoisomers of this molecular system (**1**) are depicted in Figure 9. It has been shown for molecular motors of the second generation that the helicity of the overcrowded alkene alternates between left and right handed (*M*/*P*) when rotation takes place from stable to metastable isomers with a permanent chirality (R/S) at the stereogenic center.[59] For a single atropoisomer of **1** this feature of second generation molecular motors is expressed also in its biaryl, possessing a stable absolute axial chirality (R_a/S_a) throughout the rotational cycle though alternating between a left and right handed helicity.

Results and discussion

A theoretical study was undertaken *a priori* to verify the design as shown in Figure 9, especially the delicate balance between the barrier for thermal biaryl rotation and thermal helix inversion. Furthermore, it was used to obtain the estimated temperature ranges in which the thermal processes occur at detectable

rates, intended to define the starting points in the experimental study. The potential energy surface (PES) of the ground state of the (*S*)-isomer was constructed by scanning the torsion angle of the biaryl and the dihedral angle integral to the THI (indicated by the numbered atoms, 1-2-3-4, in *(S,P,R*$_a$*)*-**1'** in Figure 10) with the use of a semi-empirical method (PM6). The minima and transition states (TS) on the PES were re-optimized using density functional theory (DFT; B3LYP/6-31G(d,p)) and their thermochemistries were calculated at the same level (Figure 10. The calculated thermodynamic data reveal two global minima very close in energy, with both an *M*-helicity over the overcrowded alkene, but opposite conformations over the biaryl moiety (Table 1).

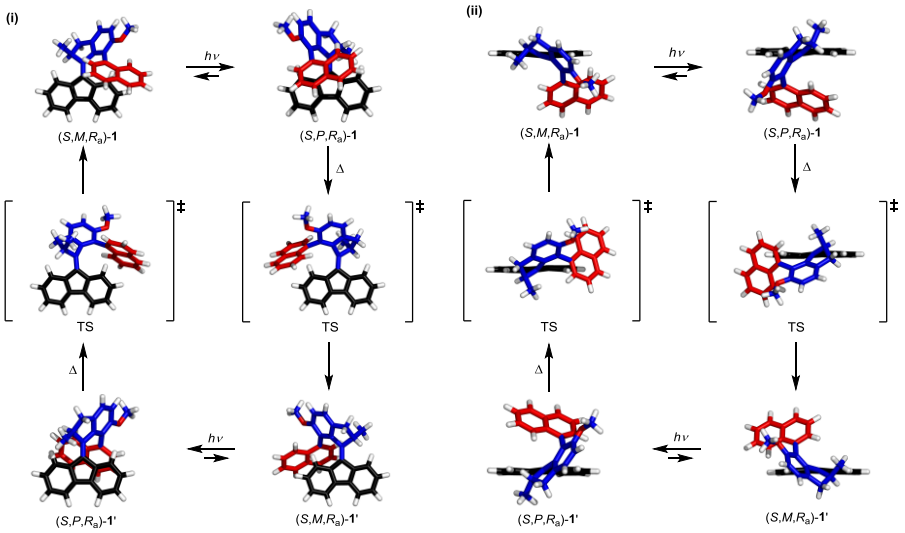

Figure 10. Rotational cycle of (*S,M,R*$_a$)-**1**. (i) Front view; (ii) Top-down view. The naphthalene moiety (red) slides along the fluorenyl lower half (black) during the photochemical *E-Z* isomerisation (from stable (*S,M,R*$_a$)-**1** to metastable *(S,P,R*$_a$)-**1**), followed by rotating around the fluorenyl in a synchronous fashion during the thermal helix inversion via the depicted TS (from metastable *(S,P,R*$_a$)-**1** to stable (*S,M,R*$_a$)-**1'**).The geometries of the minima and transition states were optimized using DFT B3LYP/6-31G(d,p)

Table 1. Calculated Gibbs free energies of motor 1 (DFT/B3LYP/631G-(d,p)).

	ΔG° (kJ·mol^{-1}) [a]	Δ‡G° (kJ·mol^{-1}) [a]
Metastable-(*S*,*P*,R_a)-**1**	11.95	
TS_{THI}-(*S*,R_a)-**1**‡	79.82	67.87
Stable-(*S*,*M*,R_a)-**1**	0.0	
TS_{BR}-(*S*,*M*,*sp*)-**1**‡	111.7	111.7
TS_{BR}-(*S*,*M*,*ap*)-**1**‡	124.1	124.1
Stable-(*S*,*M*,S_a)-**1**	1.134	
TS_{THI}-(*S*,S_a)-**1**‡	85.69	71.41
Metastable-(*S*,*P*,S_a)-**1**	14.28	
TS_{BR}-(*S*,*P*,*sp*)-**1**‡	136.6	124.6
TS_{BR}-(*S*,*P*,*ap*)-**1**‡	155.9	144.0

[a] Standard condition: 20 °C and atmospheric pressure.

The conformation stable-(*S*,*M*,R_a)-**1** with the naphthyl group in a synclinal orientation (Figure 9R_a, i.e. pointing away from the overcrowded alkene, oxygen takes priority) is predicted to be slightly in excess (2:1 at equilibrium) with respect to its atropoisomer with the naphthyl group in an anticlinal orientation (stable-(*S*,*M*,S_a)-**1**). These atropoisomers can interconvert through a BR during which the geometry goes through periplanar conformations over the biaryl bond. The barrier for synperiplanar BR (TS_{BR}-(*S*,*M*,*sp*)-**1**‡), during which the hydrogen on the C8 of naphthyl passes the methoxy group, is significantly lower than that of the antiperiplanar BR (TS_{BR}-(*S*,*M*,*ap*)-**1**‡), in which the naphthyl moiety comes in close proximity of the overcrowded alkene. However, at room temperature this atropoisomerization process is calculated to exhibit a half-life exceeding 40 days, and therefore imparts a reasonable stability to the atropoisomers. The scans along the 1-2-3-4 dihedral starting from the two stable atropoisomers revealed in each case a corresponding local minimum connected by a transition state. These local minima correspond to the characteristic metastable states of molecular motors in which the helicity is inverted with respect to the stable state and can experimentally be obtained by a photochemical *E*-*Z* isomerization.[62] Several features were revealed in the

metastable state, with respect to the corresponding stable state: (i) the helicity over the chromophores is inverted, (ii) the absolute chirality over the biaryl is preserved and, (iii) the clinal orientation of the naphthyl moiety is inverted (e.g. stable-(*S*,*M*,R_a,*sc*)-**1** gives metastable-(*S*,*P*,R_a,*ac*)-**1**, in which the descriptors for the clinal orientation are redundant and therefore otherwise omitted). A single TS connects each local minimum to its corresponding global minimum during which the naphthyl group slides around the fluorenyl moiety through a 90 degrees torsion angle over the biaryl (i.e. inverting its syn- or anticlinal conformation). This allows the chromophore to invert its helicity and this process is therefore identified as the THI. The barriers for THI were found to be very low compared to those for BR, and would result in predicted half-lives of less than 1 second at room temperature. This indicates that in order to effect a measurable lifetime of the metastable state of about 1 hour, one would need to lower the temperature to roughly -50 °C. At such a temperature the lifetime of the stable state with respect to atropoisomerization of the biaryl moiety is predicted to exceed thousands of years, which renders this undesired process completely negligible. These computational results confirm the presence of the desired features for the thermal behavior of a 'tidally locked' system. Interestingly, a design with considerable less steric bulk on the aryl moiety (R^1 = OMe, R^2 = *o*-OMe, R^3 = −, Figure 7) was also considered and as expected, computations revealed a lower barrier for BR with respect to that of **1**. However, the barrier for THI as well as the geometry of the TS was very comparable to that of **1**, which appears to be a consequence of the synchronous rotation around the biaryl bond in order to minimize steric repulsion (Figure 10), reaffirming the viability of the overall design to function as a 'tidally locked' system.

The preparation of the motor **1** started with bromination of the indanone **2** using NBS in acetonitrile to provide the brominated ketone **3** (Scheme 2). While screening several conditions for the Suzuki coupling with naphthalene-1-boronic acid, it was found that the reaction catalyzed by Pd_2dba_3 and SPhos[63] as a ligand gave the biarylketone **4** in a superior yield, and only a very small amount of the dehalogenated starting material was observed. Methylation of the ketone **5** and subsequent reaction with $NH_2NH_2.H_2O$ catalyzed by $Sc(OTf)_3$ afforded the hydrazone **6**. The hindered double bond was constructed in a classical fashion using the Barton-Kellogg coupling. The required diazo species was prepared from hydrazone **6** by oxidation in situ with MnO_2 and was immediately combined with 9*H*-fluorene-9-thione. The resulting episulfide **7** was directly subjected to a desulphurization reaction with

hexamethyltriamidophosphite (HMPT). In this manner, the desired motor **1** was formed in 49% yield (over the 3 steps) as a mixture of two atropoisomers in their thermodynamic ratio (3:1) according to ^{1}H NMR spectroscopy, assigned as (*S**,*M**,*R*a*)-**1** and (*S**,*M**,*S*a*)-**1** (for the stereochemical assignment *vide infra*). Three crystallizations from ethanol furnished the major isomer (*S**,*M**,*R*a*)-**1**.

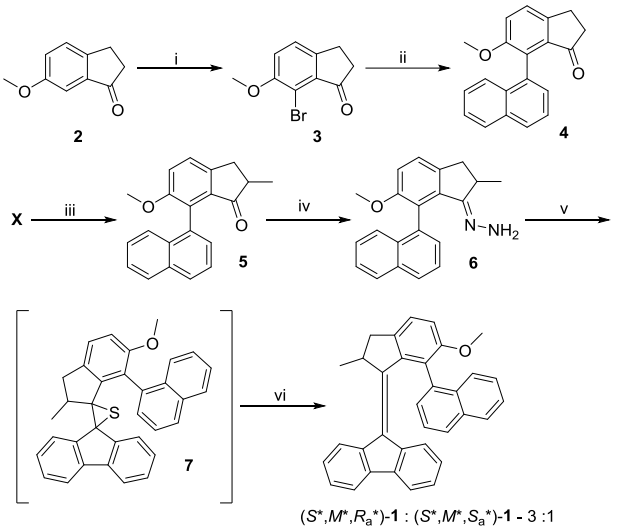

Scheme 2. Reagents and conditions: (i) NBS, MeCN, 56%; (ii) Naphthalene-1-boronic acid, Pd_2dba_3, SPhos, K_3PO_4, toluene, reflux, 16 h, 84%; (iii) LDA, MeI, THF, -78 °C, 16 h, 64%; (iv) $NH_2NH_2.H_2O$, $Sc(OTf)_3$, EtOH, reflux, 16 h, 86%; (v) 1. PIFA; 2. 9*H*-fluorene-9-thione, DMF, -50 °C to rt, 16 h; (vi) HMPT, toluene, 100 °C, 16 h, 49% over 3 steps.

Prior to conducting a study of the photochemical behavior of motor **1**, it was necessary to unequivocally determine the conformation over the single bond of the biaryl unit. As shown by DFT calculations (*vide supra*, Figure 10), we expect two isomers: one with the naphthyl in a synclinal orientation ((*S**,*M**,*R*a*)-**1**) and another with the naphthyl in an anticlinal orientation ((*S**,*M**,*S*a*)-**1**). Comparison of the experimental ^{1}H NMR of the major isomer and the calculated spectrum (ωB97XD/6-31+G(d,p)//mPW1PW91/6-311+G(2d,p)/SMD=$CHCl_3$) of **1** shows a much stronger correlation with (*S**,*M**,*R*a*)-**1** than with (*S**,*M**,*S*a*)-**1**. This correlation is especially obvious for H^{15} and H^{16} which experience the ring current of the adjacent naphthalene in the synclinal orientation, shifting the signals upfield to 5.90 and 6.61 ppm, respectively (Figure 11). The minor isomer exhibits an ^{1}H NMR spectrum without resonances characteristic for H^{15} and H^{16} shielded by the naphthyl unit and is assigned (*S**,*M**,*S*a*)-**1**.

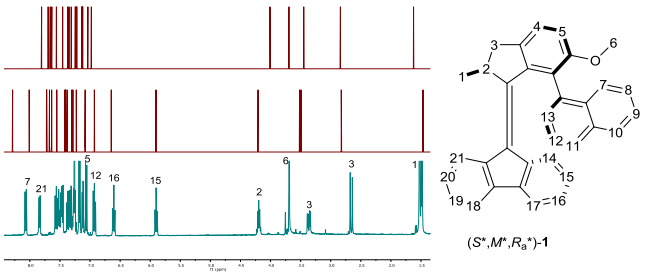

Figure 11. ^{1}H NMR ($CDCl_3$, 400 MHz). Top: calculated spectrum of the (*S**,*M**,*S*a*)-**1**; middle: calculated spectrum of the (*S**,*M**,*R*a*)-**1**; bottom: experimental spectrum of (*S**,*M**,*R*a*)-**1**; small amount (<4%) of minor (*S**,*M**,*S*a*)-**1** is present.

Unequivocal proof of the structure of the major isomer **1**, the pseudo-axial orientation of the methyl substituent at the stereogenic center and the synclinal conformation was obtained from an X-ray analysis of the crystal of the major isomer grown by slow evaporation from CH_2Cl_2/MeOH/pentane (Figure 12). The dihedral angle over the biaryl determined from the X-ray structure was found to be 62.4° and is in very good agreement with the calculated value of 60.5°.

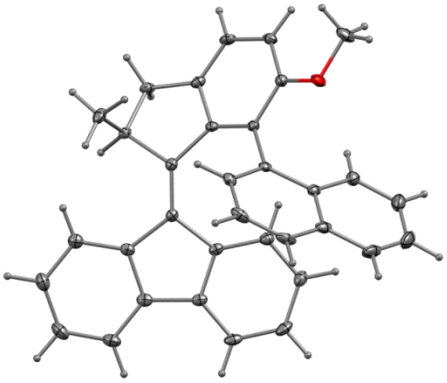

Figure 12. X-ray structure of (*S**,*M**,*R*a*)-**1**

The barrier for biaryl rotation was determined using ^{1}H-NMR spectroscopy by following the integrals of several NMR absorptions (H^1 and H^2) over time at elevated temperatures (75–95 °C) in d_8-toluene (Figure 16 and 17). An Eyring analysis provided the energies of activation ($\Delta^{\ddagger}H°_{biaryl}$ 101.1±0.6 kJ.mol^{-1}, $\Delta^{\ddagger}S°_{biaryl}$ -33.0±1.6 J.K^{-1}.mol^{-1}, $\Delta^{\ddagger}G°_{biaryl}$ 110.8±0.7 kJ.mol^{-1}, $t_{½}$(363K) 28.3±0.3 min) which are in good agreement with the calculated barrier (*vide supra*, $\Delta^{\ddagger}G°_{calc}$ =

111.6 kJ.mol^{-1}) and the half-life for this process at room temperature which corresponds to about 75 days.

In order to verify that the ability to perform photochemically driven rotation remained uncompromised, the photochemical and thermal isomerization processes were followed by UV-vis spectroscopy. Irradiation of (*S**,*M**,*R*$_a$*)-**1** with ultraviolet light (365 nm, heptane) at −60 °C resulted in the emergence of a bathochromically shifted absorption band consistent with the behavior of other second generation motors and indicative of an increase in alkene strain as is expected for the metastable form (*S**,*P**,*R*$_a$*)-**1** (Figure 13, blue dotted).[64] After the photostationary state (PSS) was reached, the sample was allowed to reach room temperature and full reversal to the original UV-vis spectrum was observed, indicating the anticipated thermal helix inversion is taking place (Figure 13, red dashed). Both processes proceeded with an isosbestic point at 393 nm. Following this thermal process over time at various temperatures between -65 °C and -45 °C using UV-vis spectroscopy allowed for construction of an Eyring plot and derivation of the respective energies of activation ($\Delta^{\ddagger}H°_{THI}$ 34.5±0.5 kJ.mol^{-1}, $\Delta^{\ddagger}S°_{THI}$ -143.3±2.3 J.K^{-1}.mol^{-1}, $\Delta^{\ddagger}G°_{THI}$ 76.6±0.8 kJ.mol^{-1}, $t_{½}$ at rt 5.4±1.8 s), in good agreement with the calculated barrier ($\Delta^{\ddagger}G_{exp}$ (-50 °C) = 66.5 kJ mol^{-1} , $\Delta^{\ddagger}G_{calc}$ (-50 °C) = 65.9 kJ.mol^{-1}).[65]

The experimental values of the barriers for both the biaryl rotation and thermal helix inversion confirmed that the required condition ($\Delta^{\ddagger}G°_{biaryl} > \Delta^{\ddagger}G°_{THI}$) for synchronous motion (*vide supra*) had been fulfilled as predicted by calculations.

The propensity to undergo biaryl motion coupled to the rotary motion of the molecular motor as proposed following our molecular design was assessed at this point using ^{1}H NMR and CD spectroscopy.

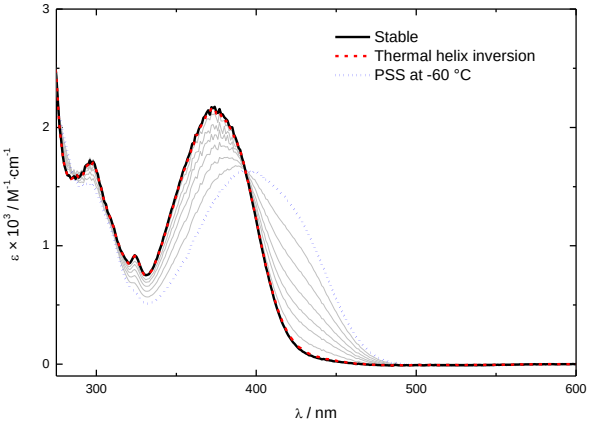

Figure 13. UV-vis absorption spectrum of (*S**,*M**,*R*a*)-**1** in heptane at -60 °C (black solid); irradiation (365 nm) to PSS at -60 °C (dotted blue); and after warming to room temperature measured at -60 °C (dashed red).

Independent NMR spectroscopy experiments confirmed that irradiation (365 nm, d_8-toluene) of (*S**,*M**,*R*a*)-**1** at -80 °C produces an additional species which lacks NMR absorptions at 6.09, 6.53, 8.00 and 7.86 ppm (belonging to H^{15}, H^{16}, H^{7} and H^{21}, of (*S**,*M**,*R*a*)-**1**, respectively) and two new absorptions at 7.60 and 7.73 ppm are observed (Figure 14ii). This observation is consistent with formation of the anticipated metastable (*S**,*P**,*R*a*)-**1** in which the naphthalene moiety adopts an anticlinal orientation thus moving away from the vicinity of the H^{15} and H^{16}, disturbing the effects of the ring current on the aforementioned protons. The original ^{1}H NMR spectrum of (*S**,*M**,*R*a*)-**1** is completely recovered upon heating the sample back to room temperature demonstrating that the conformation of the biaryl is indeed retained after one half of the rotational cycle (Figure 14iii). The efficiency of this synchronous motion has been further probed by irradiation (365 nm, CD_2Cl_2) of a sample of racemic (*S**,*M**,*R*a*)-**1** at room temperature for 24 hours. The initial ratio of (*S**,*M**,*R*a*)-**1** and (*S**,*M**,*S*a*)-**1** remained unchanged in the process, manifesting the efficiency of the process across multiple photochemical cycles. Note that 20 °C is much too low for this system to allow the biaryls to return to their thermodynamic equilibrium ($t_{½}$ at rt 75 d, *vide supra*).

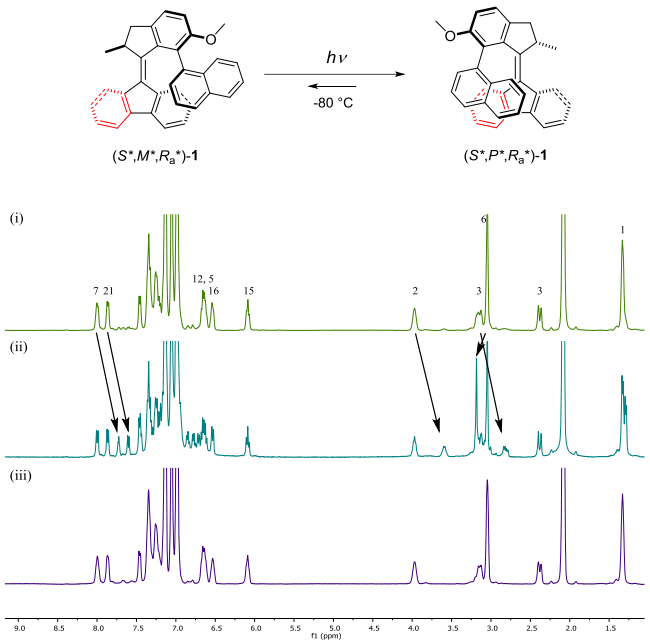

Figure 14. (top) Irradiation of (S^*,M^*,R_a^*)-**1** at -80 °C to produce metastable (S^*,P^*,R_a^*)-**1**. (bottom) ^{1}H NMR spectra (d_8-toluene, 400 MHz, -55 °C): (i) (S^*,M^*,R_a^*)-**1** with proton assignments (Figure 11) depicted on top; (ii) after irradiation (365 nm) at -80 °C for 3 h; appearance of the metastable (S^*,P^*,R_a^*)-**1** is denoted by arrows; (iii) after warming to room temperature for 10 min (for assignment of signals see Figure 11).

To gain more insight in the dynamic behavior of the naphthalene moiety, the rotational cycle was followed by CD spectroscopy. For this purpose, a single enantiomer (*R*,*P* or *S*,*M*) of each atropoisomer (R_a and S_a) of motor **1** was isolated using preparative supercritical fluid chromatography (SFC) on a chiral stationary phase (Chiralpak IA, 18% MeOH in CO_2, 3.0 ml min^{-1}, T = 40 °C, 180 bar). In order assign the absolute stereochemistry of the stereogenic center, the biaryl and the helicity of the separated isomers, the experimentally obtained CD-spectra were compared to calculated CD-spectra obtained by time dependent DFT (TD-DFT/ B3LYP/6-31G(d,p), Figure 15i and 15iii). The relative stereochemical configuration and conformation in the major isomer (Figure 14i) have been identified by X-Ray and ^{1}H NMR, while for the minor isomer (Figure 14iii) the relative configuration and conformation have been established by the experimental BR ^{1}H NMR study (Figure 16), which in both cases agreed with the computationally predicted relationship (*vide supra*). Due to this prior knowledge regarding the isomers, the comparison of CD spectra is only required to

differentiate between enantiomers. However, to allow CD spectroscopy to be an independent tool, capable of identifying all stereochemical elements in the isomers, we compared the experimental spectra to the calculated spectra of all four possible isomers (namely the stable configurations (*S*,*M*,*R*$_a$)-**1**, (*R*,*P*,*S*$_a$)-**1**, (*S*,*M*,*S*$_a$)-**1**, and (*R*,*P*,*R*$_a$)-**1**).

The two isomers (one of *R*$_a$ and one of *S*$_a$; the remaining two were inseparable) isolated by SFC clearly possess a diastereomeric relationship due to the absence of a mirror relationship between their CD-spectra (heptane, −80 °C, Figure 15i and iii). The experimental CD-spectra of the two isomers were compared to the calculated spectra which revealed a strong correlation with (*R*,*P*,*S*$_a$)-**1** in Figure 15i and with (*R*,*P*,*R*$_a$)-**1** in Figure 15iii thereby providing the absolute stereochemical assignment of the isolated isomers. The experimental CD spectrum of (*R*,*P*,*S*$_a$)-**1** (with the naphthyl moiety in a synclinal orientation) possesses distinct absorption bands with maxima at 299 and 399 nm, while the experimental CD spectrum of (*R*,*P*,*R*$_a$)-**1** (with the naphthyl moiety in an anticlinal orientation) shows absorptions bands at 299, 332 and 386 nm (Figure 15). Interestingly, while the CD spectrum of (*R*,*P*,*S*$_a$)-**1** only exhibits two sign inversions over the recorded region, that of (*R*,*P*,*R*$_a$)-**1** exhibits five sign inversion features, which for both isomers are also observed in the calculated CD spectra. Irradiation of separate samples of (*R*,*P*,*S*$_a$)-**1** and (*R*,*P*,*R*$_a$)-**1** with ultraviolet light (365 nm) at -80 °C provided the CD spectra of their respective PSS mixtures (Figure 15ii and 15iv). The CD-spectra of the PSS mixtures exhibit significant changes with respect to their initial configurations and an overall slight bathochromic shift was observed which is common for the metastable forms of second generation molecular motors with a fluorenyl lower half.[64] Interestingly, the PSS mixtures give absorption bands which bear a resemblance to inverted CD-spectra of the diastereoisomers of their initial stable configurations (e.g. the CD-spectrum of the PSS mixture of (*R*,*P*,*S*$_a$)-**1** (15ii) resembles that of a mirror image of (*R*,*P*,*R*$_a$)-**1** (15iii) – the mirror image of the CD-spectrum of (*R*,*P*,*R*$_a$)-**1** belongs to its enantiomer, (*S*,*M*,*S*$_a$)-**1**). This was to be expected from a 'tidally locked' system, where the helicities of the chromophores, which provide the major absorption bands, invert during the photochemical *E*-*Z* isomerization while retaining their absolute point- and axial-chirality (e.g. stable-(*R*,*P*,*S*$_a$)-**1** (15i) is expected to photo-isomerize to metastable-(*R*,*M*,*S*$_a$)-**1** (15ii) of which the helicities of the chromophores correspond to those of stable-(*S*,*M*,*S*$_a$)-**1**, see Figure 9 and Figure 15). However close the resemblance might be, the two isomers are not identical and therefore neither are their CD-

spectra, furthermore, the PSS mixtures are not pure metastable species but still contain some amount of the stable starting materials. A comparison of the CD-spectra of the PSS mixtures with the calculated CD-spectra confirmed the proposed identities of the metastable species (Figure 15ii and 15iv, and thereby confirmed the presence of tidal locking during the photochemical step.

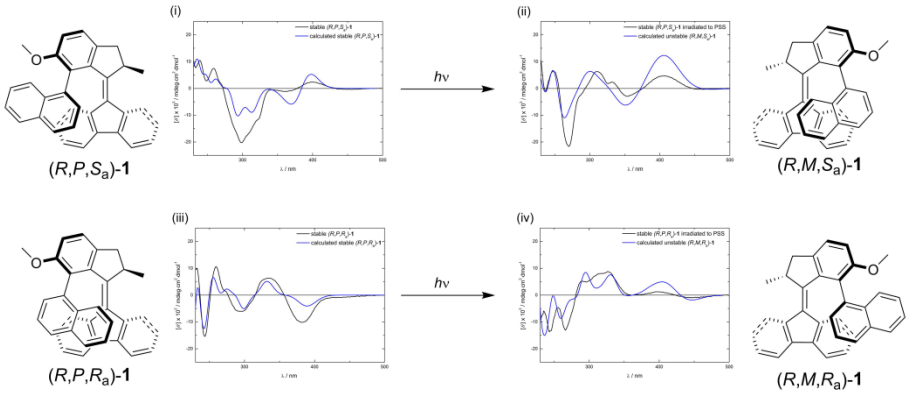

Figure 15. CD spectra (heptane, -80 °C): (i) stable (*R*,*P*,S_a)-**1** (black); calculated stable (*R*,*P*,S_a)-**1** (blue); (ii) stable (*R*,*P*,S_a)-**1** irradiated (365 nm) to PSS (black); calculated metastable (*R*,*M*,S_a)-**1** (blue); (iii) stable (*R*,*P*,R_a)-**1** (black); calculated stable (*R*,*P*,R_a)-**1** (blue); (iv) stable (*R*,*P*,R_a)-**1** irradiated (365 nm) to PSS (black); calculated metastable (*R*,*M*,R_a)-**1**. Gaussian line broadening was used to produce the spectra from the calculated transitions.

The formation of (*R*,*M*,S_a)-**1** upon irradiation of (*R*,*P*,S_a)-**1** observed in CD spectroscopy (Figure 15i to ii) is consistent with the behavior of (S^*,M^*,R_a^*)-**1** observed by ^{1}H-NMR spectroscopy (Figure 14i to ii), for which the shift of the characteristic absorptions of H^{15} and H^{16} confirmed movement of the naphthalene from synclinal to anticlinal orientation and thus the formation of (S^*,P^*,R_a^*)-**1**. In conjunction, these observations establish that suggested mode of action in the course of the photochemical *E*-*Z* isomerization is taking place. The samples containing the PSS mixtures were then allowed to warm to room temperature which brought about changes in the absorption bands providing CD-spectra identical to those of their respective starting materials (Figure 15i and iii), analogous to the recovery of the original ^{1}H NMR spectra upon heating (Figure 14iii). These findings unequivocally confirm the proposed mode of rotation for the thermal isomerization (Figure 9), during which a second helicity inversion (*M*/*P*) of the motor takes place with retention of the biaryl axial chirality (R_a/S_a), establishing that during the THI the naphthyl group rotates around the fluorenyl moiety while keeping a single side of the naphthyl group

faced towards the lower half. This clearly demonstrates that upon irradiation, the molecular motor exhibits a four stage (clockwise or counterclockwise) rotation with a concomitant sliding/rotation of the biaryl moiety.

Conclusions

In conclusion, the behavior of a molecular motor with an built-in biaryl moiety was investigated throughout the photochemically driven rotational cycle. CD and NMR spectroscopy measurements, supported by computational studies, show that the naphthalene moiety slides along the lower half in a synchronous manner during photochemical *E*-*Z* isomerization, followed by a synchronous rotation around the lower half in the process of the thermal helix inversion, retaining its conformation after each cycle. The movement essentially results in the same face of the naphthalene always facing the motor during the rotation of the molecular motor, such as in case of a chain on sprocket. Thereby, we have demonstrated that the rotational behavior of the molecular motor can be further expanded to influence systems coupled to the motor, thus opening further venues for more elaborate molecular machinery.

Experimental part

General remarks

Reagents were purchased from Aldrich, Merck or Fluka and were used as provided unless otherwise indicated. The solvents were distilled and dried, if necessary, by standard methods. Column chromatography was performed on silica gel (Merck type 9385 230-400 mesh) using positive pressure, TLC: silica gel 60, Merck, 0.25 mm. High Resolution Mass spectra (HRMS) were recorded on an LTQ Orbitrap XL. NMR spectra were obtained using a a Varian Mercury Plus (^{1}H: 400 MHz, ^{13}C: 100 MHz), a Varian Unity Plus (^{1}H: 500 MHz, ^{13}C: 125 MHz) or a Varian Innova (^{1}H: 600 MHz,) in $CDCl_3$, d_8-toluene or CD_2Cl_2. Chemical shifts are reported in δ units (ppm) relative to the residual deuterated solvent signal of $CDCl_3$ (^{1}H NMR, δ 7.26 ppm; ^{13}C NMR, δ 77.23 ppm), d_8-toluene (^{1}H NMR, δ 2.09 ppm), or CD_2Cl_2 (^{1}H NMR, δ 5.32 ppm; ^{13}C NMR, δ 54.0 ppm). The splitting patterns are designated as follows: s (singlet), d (doublet), t (triplet), q (quartet), dd (doublet of doublets), td (triplet of doublets), qt (quartet of triplets), m (multiplet) and br (broad). SFC was performed on a Thar SFC system consisting of a fluid delivery module (FDM10-1), an autosampler (a modified

Alias 840), a semi-prep column oven, PDA detector, a back pressure regulator (ABPR20), heat-exchanger, and a fraction collector (modified Thar SFC-FC). UV-vis absorption spectra were measured on a Jasco V-630 or a Hewlett-Packard 8453 spectrometer. CD spectra were measured on a Jasco J-815 CD spectrometer. Heptane used for spectroscopic studies was of spectroscopic grade (UVASOL Merck). Irradiations were performed using a spectroline ENB-280C/FE lamp (λ_{max} = 365 nm).

Synthesis

7-Bromo-6-methoxy-2,3-dihydro-1*H*-inden-1-one (3).

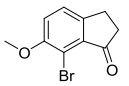

A solution of 6-methoxy-2,3-dihydro-1*H*-inden-1-one (10.0 g, 61.7 mmol) and NBS (13.2 g, 73.9 mmol) in acetonitrile (500 mL) was heated at reflux for 16 h. After cooling down to room temperature, acetonitrile was removed under reduced pressure and the residue was partitioned between CH_2Cl_2 (400 mL) and aq. NaOH (2 M, 250 mL). The organic layer was washed with water (200 mL), brine (100 mL) and dried with Na_2SO_4. The solvents were removed under reduced pressure and the residue was crystallized from EtOH (150 mL) to give the product **3**. Yield: 8.32 g (56 %); tan solid. Mp. 171.0–172.2 °C. ^{1}H NMR (400 MHz, $CDCl_3$): δ (ppm) 7.35 (d, J = 8.3 Hz, 1H), 7.14 (d, J = 8.3 Hz, 1H), 3.92 (s, 3H), 3.13–2.90 (t, J = 6.2 Hz, 2H), 2.84–2.64 (m, 2H). ^{13}C NMR (100 MHz, $CDCl_3$): δ (ppm) 204.1, 155.6, 149.2, 135.2, 125.9, 118.2, 108.3, 57.0, 37.8, 23.9. HRMS (ESI+): calcd for $C_{10}H_{10}BrO_2^+$ [M + H$^+$] 240.9858 found 240.9876.

6-Methoxy-7-(naphthalen-1-yl)-2,3-dihydro-1*H*-inden-1-one (4).

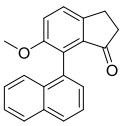

A solution of **3** (6.0 g, 24.9 mmol), naphthalene-1-boronic acid (6.41 g, 37.3 mmol) Pd_2dba_3 (228 mg, 0.25 mmol), SPhos (408 mg, 1.0 mmol) and K_3PO_4 (15.8 g, 74.7 mmol) in dry toluene (70 mL) was degassed by bubbling with nitrogen gas for 15 min. The resulting mixture was heated at reflux overnight, cooled down and filtered through a pad of Celite (3 × 1 cm). The Celite pad was washed with ethyl acetate (2 × 40 mL) and the filtrate was concentrated under reduced pressure. The residue was purified by column chromatography (pentane : ethyl acetate – 15 : 1) to provide the title compound. Yield: 5.74 g (80 %); white solid. Mp. 114.2–117.7 °C. ^{1}H NMR (400 MHz, $CDCl_3$): δ (ppm) 7.91 (d, J = 7.9 Hz, 2H), 7.56 (dd, J_1 = 7.2 Hz, J_2 = 7.1 Hz, 1H), 7.54 (dd, J_1 = 7.3 Hz, J_2 = 7.2 Hz, 1H), 7.44 (m, 1H), 7.30–7.37 (m, 4H), 3.68 (s, 3H), 3.12 (t, J = 6.1 Hz, 2H), 2.62 (dt, J_1 = 6.2 Hz J_2 = 1.8 Hz, 2H). ^{13}C NMR (100

MHz, $CDCl_3$): δ (ppm) 205.3, 157.0, 147.6, 136.3, 133.6, 132.7, 132.4, 128.5, 128.0, 127.1, 127.09, 126.9, 125.8, 125.52, 125.51, 125.4, 118.2, 56.9, 37.6, 24.7. HRMS (ESI+): calcd for $C_{20}H_{17}O_2^+$ [M + H^+] 289.1223 found 289.1220.

6-Methoxy-2-methyl-7-(naphthalen-1-yl)-2,3-dihydro-1*H*-inden-1-one (5).

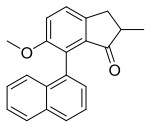

To a solution of diisopropylamine (807 mg, 1.11 mL, 7.98 mmol) in dry THF (30 mL) at -78 °C, *n*-BuLi (5.0 mL, 7.98 mmol, 1.6 M in hexane) was added dropwise over 10 min. After stirring for 15 min, a solution of **4** (2.0 g, 6.94 mmol) in dry THF (20 mL) was added dropwise over 5 min. The resulting solution was left stirring for 1 h at -78 °C and subsequently methyl iodide (1.13 g, 498 µl, 7.98 mmol) was added at once. The mixture was left to warm overnight, quenched by addition of water (15 ml) and extracted with CH_2Cl_2 (3 x 50 ml). The combined organic layers were dried with anhydrous Na_2SO_4 and the solvents were removed under reduced pressure. The residue was purified by column chromatography (pentane : ethyl acetate – 15 : 1) to give the desired compound as a mixture of atropoisomers (~1:1). Yield: 1.28 g (61 %); white solid. Mp. 136.7–138.2 °C. ^{1}H NMR (400 MHz, $CDCl_3$): δ (ppm) 7.88 (d, 2H, J = 8.2 Hz), 7.46–7.59 (m, 2H), 7.38–7.45 (m, 1H), 7.27–7.35 (m, 4), 3.68 (m, 3H), 3.38 (dd, J_1 = 16.4 Hz, J_2 = 8.0 Hz, 1H), 2.59–2.70 (m, 2H), 1.14–1.22 (m, 3H). ^{13}C NMR (100 MHz, $CDCl_3$): δ (ppm) 207.82, 207.79, 157.1, 145.78, 145.77, 133.64, 133.59, 132.8, 132.6, 132.5, 132.4, 128.6, 128.1, 128.0, 127.3, 127.0, 126.71, 126.70, 125.80, 125.77, 125.7, 125.59, 125.55, 125.4, 118.3, 118.1, 56.92, 56.86, 43.5, 43.3, 34.0, 16.3, 16.1. HRMS (ESI+): calcd for $C_{21}H_{19}O_2^+$ [M + H^+] 303.1380 found 303.1377.

9-(6-Methoxy-2-methyl-7-(naphthalen-1-yl)-2,3-dihydro-1*H*-inden-1-ylidene)-9*H*-fluorene (1).

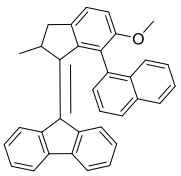

Hydrazine monohydrate (20 mL) was added to a solution of **5** (1.5 g mg, 4.96 mmol) and $Sc(OTf)_3$ (73 mg, 0.15 mmol) in EtOH (20 mL) at room temperature. The resulting mixture was heated at reflux overnight. After cooling down, water (40 mL) was added and the mixture was extracted with CH_2Cl_2 (3 × 50 ml). The combined organic layers were washed with water (2 × 50 mL), dried with anhydrous Na_2SO_4 and the solvents were removed under reduced pressure to give the hydrazone **6** compound as a complex mixture of atropoisomers and geometric isomers. Yield: 1.35 mg (86%); pale yellow solid. The material was used without further purification.

A solution of **6** (400 mg, 1.26 mmol) in dry DMF (10 mL) was cooled down to -50 °C. [Bis(trifluoroacetoxy)iodo]benzene (598 mg, 1.39 mmol) in dry DMF (1 mL) was added dropwise to the mixture. After stirring the mixture for 1 min, a solution of 9*H*-fluorene-9-thione (370 mg, 1.89 mmol) in CH_2Cl_2 (5 mL) was added dropwise over 5 min. The mixture was left to warm overnight, the solvents were evaporated under reduced pressure and the residue was redissolved in toluene (20 mL). HMPT (460 µL, 411 mg, 2.52 mmol) was added and the mixture was heated at reflux overnight. The solvents were evaporated under reduced pressure. The residue purified by column chromatography (pentane : ethyl acetate – 20 : 1), followed by three crystallizations from EtOH to yield the product as a single atropoisomer (*S*,M*,R*$_a$*)-**1**. Yield of mixture of atropoisomers: 278 mg (49 %); pale yellow solid. (*S*,M*,R*$_a$*)-**1**: Mp. >250 °C (decomp.). ^{1}H NMR (400 MHz, $CDCl_3$): δ (ppm) 8.07 (d, J = 8.5 Hz, 1H), 7.84 (d, J = 6.9 Hz, 1H), 7.57 (d, J = 8.1 Hz, 1H), 7.43–7.55 (m, 3H), 7.22–7.39 (m, 4H), 7.18 (d, J = 7.7 Hz, 2H), 7.12 (d, J = 7.1 Hz, 1H), 7.06 (d, J = 8.2 Hz, 1H), 6.93 (dd, J_1 = 7.7 Hz, J_2 = 7.7 Hz, 1H), 6.61 (dd, J_1 = 7.5 Hz, J_2 = 7.5 Hz, 1H), 5.90 (dd, J_1 = 7.6 Hz, J_2 = 7.6 Hz, 1H), 4.20 (m, 1H), 3.69 (s, 3H), 3.36 (dd, J_1 = 14.0 Hz, J_2 = 5.8 Hz, 1H), 2.66 (d, J = 14.0 Hz, 1H), 1.49 (d, J = 6.7 Hz, 3H). ^{13}C NMR (100 MHz, $CDCl_3$): δ (ppm) 156.3, 149.8, 142.1, 141.2, 140.4, 139.8, 138.2, 135.9, 135.0, 133.7, 131.8, 131.3, 129.04, 128.99, 128.5, 128.1, 127.9, 127.0, 126.6, 126.5, 126.2, 125.1, 125.02, 124.99, 124.9, 124.7, 124.2, 119.6, 117.6, 112.4, 56.0, 45.7, 41.0, 18.6. HRMS (ESI+): calcd for $C_{34}H_{27}O^+$ [M + H$^+$] 451.2056 found 451.2044.

Kinetic measurements

Biaryl barrier: NMR samples in d_8-toluene were heated (75–95°C) inside a Varian Innova 600 NMR with the temperatures controlled with a PT-100 resistance thermometer. ^{1}H NMR absorptions of H1 and H2 were followed at 3 min intervals (Figure 16) and a least square fitting of the trace (Figure 17) to a first order formation afforded the reaction rates from which an Eyring plot was constructed. A least squares analysis was performed on the linearized form of the Eyring equation.

THI barrier: UV-vis samples in heptane (~2 × 10^{-5} M) were irradiated with a spectroline ENB-280C/FE lamp (λ_{max} = 365 ± 30 nm) at -48 to -68 °C to reach PSS. The thermal helix inversion was followed by recording UV-vis spectra at 30–120 sec intervals and multivariate analysis was performed across the array of spectra in order to extract the rate constants used to construct the Eyring plot. A least squares analysis was performed on the linearized form of the Eyring equation.

Irradiation experiments analyzed by ^{1}H NMR spectroscopy: A solution of (*S*,M*,R$_a$**)-**1** (2 mg) in d_8-toluene (0.5 mL) was irradiated with ENB-280C/FE lamp (λ_{max} = 365 nm) in acetone-N_2(*l*) bath at -85 °C for 3 h and then transferred into a Varian Mercury Plus 400 pre-cooled to -55 °C.

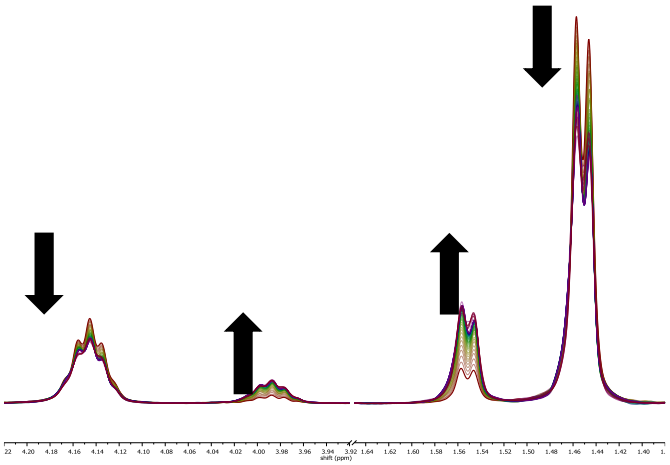

Figure 16. ^{1}H NMR (d_8–toluene, 600 MHz): Example of isomerisation of (*S*,M*,R$_a$**)-**1** into (*S*,M*,S$_a$**)-**1** measured at 85 °C over 3 h. Measurements were taken at 3 min intervals.

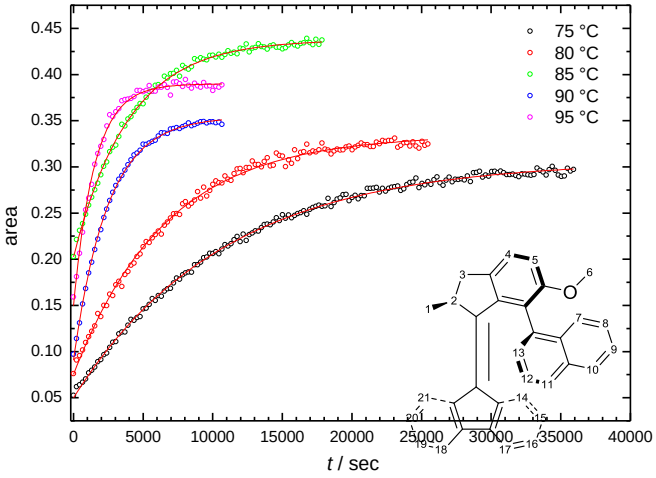

Figure 17. Thermal behavior of (*S*,M*,R$_a$**)-**1**. Integral ratio of the ^{1}H NMR absorptions of the sum of H1$_{(S^*,M^*,Sa^*)\text{-}1}$ and H2$_{(S^*,M^*,Sa^*)\text{-}1}$ over the sum of H1$_{(S^*,M^*,Ra^*)\text{-}1}$ and H2$_{(S^*,M^*,Ra^*)\text{-}1}$ over time (d_8–toluene, 600MHz, 75–95 °C). The inset shows proton assignment of (*S*,M*,R$_a$**)-**1**.

References

(1) Schliwa, M. *Molecular motors*; VCH-Wiley, 2006.
(2) Browne, W. R.; Feringa, B. L. *Nat. Nanotechnol.* **2006**, *1* (1), 25.
(3) Stoddart, J. F. *Chem. Soc. Rev.* **2009**, *38* (6), 1802.
(4) Gu, H.; Chao, J.; Xiao, S.-J.; Seeman, N. C. *Nature* **2010**, *465* (7295), 202.
(5) Kudernac, T.; Ruangsupapichat, N.; Parschau, M.; Maciá, B.; Katsonis, N.; Harutyunyan, S. R.; Ernst, K.-H.; Feringa, B. L. *Nature* **2011**, *479* (7372), 208.
(6) Cha, T.-G.; Pan, J.; Chen, H.; Salgado, J.; Li, X.; Mao, C.; Choi, J. H. *Nat. Nanotechnol.* **2014**, *9* (1), 39.
(7) Kottas, G. S.; Clarke, L. I.; Horinek, D.; Michl, J. *Chem. Rev.* **2005**, *105* (4), 1281.
(8) Kinbara, K.; Aida, T. *Chem. Rev.* **2005**, *105* (4), 1377.
(9) Kistemaker, J. C. M.; Štacko, P.; Visser, J.; Feringa, B. L. *Nat. Chem.* **2015**, *7* (11), 890.
(10) García-López, V.; Chiang, P.-T.; Chen, F.; Ruan, G.; Martí, A. A.; Kolomeisky, A. B.; Wang, G.; Tour, J. M. *Nano Lett.* **2015**, *15* (12), 8229.
(11) Tierney, H. L.; Murphy, C. J.; Jewell, A. D.; Baber, A. E.; Iski, E. V; Khodaverdian, H. Y.; McGuire, A. F.; Klebanov, N.; Sykes, E. C. H. *Nat. Nanotechnol.* **2011**, *6* (10), 625.
(12) von Delius, M.; Geertsema, E. M.; Leigh, D. A. *Nat. Chem.* **2010**, *2* (2), 96.
(13) Bissell, R. A.; Córdova, E.; Kaifer, A. E.; Stoddart, J. F. *Nature* **1994**, *369* (6476), 133.
(14) Coskun, A.; Banaszak, M.; Astumian, R. D.; Stoddart, J. F.; Grzybowski, B. A. *Chem. Soc. Rev.* **2012**, *41* (1), 19.
(15) Kassem, S.; Lee, A. T. L.; Leigh, D. A.; Markevicius, A.; Solà, J. *Nat. Chem.* **2015**, *8* (2), 138.
(16) Sauvage, J.-P. *Molecular Machines and Motors. Structure and Bonding*; Springer-Verlag Berlin Heidelberg, 2001.
(17) Balzani, V.; Credi, A.; Venturi, M. *Molecular Devices and Machines - Concepts and Perspectives for the Nanoworld*; VCH-Wiley, 2008.
(18) Balzani, V.; Credi, A.; Venturi, M. *Molecular Devices and Machines– A Journey into the Nano World*; Wiley-VCH Verlag GmbH & Co. KGaA: Weinheim, FRG, 2003.
(19) Erbas-Cakmak, S.; Leigh, D. A.; McTernan, C. T.; Nussbaumer, A. L. *Chem. Rev.* **2015**, *115* (18), 10081.
(20) Kay, E. R.; Leigh, D. A. *Angew. Chemie Int. Ed.* **2015**, *54* (35), 10080.
(21) Flood, A. H.; Stoddart, J. F.; Steuerman, D. W.; Heath, J. R. *Science* **2004**, *306* (5704), 2055.
(22) Collier, C. P. *Science (80-.).* **2000**, *289* (5482), 1172.
(23) de Silva, P. A.; Gunaratne, N. H. Q.; McCoy, C. P. *Nature* **1993**, *364* (6432),

42.
(24) Raymo, F. M. *Adv. Mater.* **2002**, *14* (6), 401.
(25) Ferris, D. P.; Zhao, Y.-L.; Khashab, N. M.; Khatib, H. A.; Stoddart, J. F.; Zink, J. I. *J. Am. Chem. Soc.* **2009**, *131* (5), 1686.
(26) Kocer, A. *Science (80-.).* **2005**, *309* (5735), 755.
(27) Berná, J.; Leigh, D. A.; Lubomska, M.; Mendoza, S. M.; Pérez, E. M.; Rudolf, P.; Teobaldi, G.; Zerbetto, F. *Nat. Mater.* **2005**, *4* (9), 704.
(28) Angelos, S.; Yang, Y.-W.; Patel, K.; Stoddart, J. F.; Zink, J. I. *Angew. Chem. Int. Ed. Engl.* **2008**, *47* (12), 2222.
(29) Li, Q.; Fuks, G.; Moulin, E.; Maaloum, M.; Rawiso, M.; Kulic, I.; Foy, J. T.; Giuseppone, N. *Nat. Nanotechnol.* **2015**, *10* (2), 161.
(30) Bruns, C. J.; Stoddart, J. F. *Acc. Chem. Res.* **2014**, *47* (7), 2186.
(31) Jiménez, M.; Dietrich-Buchecker, C.; Sauvage, J. *Angew. Chem. Int. Ed. Engl.* **2000**, *39* (18), 3284.
(32) Chen, K.-Y.; Ivashenko, O.; Carroll, G. T.; Robertus, J.; Kistemaker, J. C. M.; London, G.; Browne, W. R.; Rudolf, P.; Feringa, B. L. *J. Am. Chem. Soc.* **2014**, *136* (8), 3219.
(33) Lewandowski, B.; De Bo, G.; Ward, J. W.; Papmeyer, M.; Kuschel, S.; Aldegunde, M. J.; Gramlich, P. M. E.; Heckmann, D.; Goldup, S. M.; D'Souza, D. M.; Fernandes, A. E.; Leigh, D. A. *Science* **2013**, *339* (6116), 189.
(34) Wang, J.; Feringa, B. L. *Science* **2011**, *331* (6023), 1429.
(35) Stoll, R. S.; Hecht, S. *Angew. Chem. Int. Ed. Engl.* **2010**, *49* (30), 5054.
(36) Boyer, P. D. *Nature* **1999**, *402* (6759), 247.
(37) Berg, H. C.; Anderson, R. A. *Nature* **1973**, *245* (5425), 380.
(38) Frantz, D. K.; Linden, A.; Baldridge, K. K.; Siegel, J. S. *J. Am. Chem. Soc.* **2012**, *134* (3), 1528.
(39) Öki, M. *Angew. Chemie Int. Ed. English* **1976**, *15* (2), 87.
(40) Setaka, W.; Nirengi, T.; Kabuto, C.; Kira, M. *J. Am. Chem. Soc.* **2008**, *130* (47), 15762.
(41) Sanada, K.; Ube, H.; Shionoya, M. *J. Am. Chem. Soc.* **2016**, *138* (9), 2945.
(42) Hounshell, W. D.; Johnson, C. A.; Guenzi, A.; Cozzi, F.; Mislow, K. *Proc. Natl. Acad. Sci. U. S. A.* **1980**, *77* (12), 6961.
(43) Johnson, C. A.; Guenzi, A.; Mislow, K. *J. Am. Chem. Soc.* **1981**, *103* (16), 6240.
(44) Chance, J. M.; Geiger, J. H.; Okamoto, Y.; Aburatani, R.; Mislow, K. *J. Am. Chem. Soc.* **1990**, *112* (9), 3540.
(45) Koga, N.; Kawada, Y.; Iwamura, H. *J. Am. Chem. Soc.* **1983**, *105* (16), 5498.
(46) Chance, J. M.; Geiger, J. H.; Okamoto, Y.; Aburatani, R.; Mislow, K. *J. Am. Chem. Soc.* **1990**, *112* (9), 3540.
(47) Koga, N.; Kawada, Y.; Iwamura, H. *Tetrahedron* **1986**, *42* (6), 1679.
(48) Frantz, D. K.; Linden, A.; Baldridge, K. K.; Siegel, J. S. *J. Am. Chem. Soc.* **2012**, *134* (3), 1528.

(49) ter Wiel, M. K. J.; Feringa, B. L. *Tetrahedron* **2009**, *65* (22), 4332.
(50) Hounshell, W. D.; Iroff, L. D.; Iverson, D. J.; Wroczynski, R. J.; Mislow, K. *Isr. J. Chem.* **1980**, *20*, 65.
(51) Hounshell, W. D.; Iroff, L. D.; Wroczynski, R. J.; Mislow, K. *J. Am. Chem. Soc.* **1978**, *100* (16), 5212.
(52) Clayden, J.; Pink, J. H. *Angew. Chemie Int. Ed.* **1998**, *37* (13–14), 1937.
(53) Siegel, J.; Gutierrez, A.; Schweizer, W. B.; Ermer, O.; Mislow, K. *J. Am. Chem. Soc.* **1986**, *108* (7), 1569.
(54) Ogi, S.; Ikeda, T.; Wakabayashi, R.; Shinkai, S.; Takeuchi, M. *Chem. - A Eur. J.* **2010**, *16* (28), 8285.
(55) Liu, S.; Kondratuk, D. V.; Rousseaux, S. A. L.; Gil-Ramírez, G.; O'Sullivan, M. C.; Cremers, J.; Claridge, T. D. W.; Anderson, H. L. *Angew. Chemie - Int. Ed.* **2015**, *54* (18), 5355.
(56) Romeo, R.; Carnabuci, S.; Fenech, L.; Plutino, M. R.; Albinati, A. *Angew. Chemie - Int. Ed.* **2006**, *45* (27), 4494.
(57) Sanada, K.; Ube, H.; Shionoya, M. *J. Am. Chem. Soc.* **2016**, *138* (9), 2945.
(58) Setaka, W.; Nirengi, T.; Kabuto, C.; Kira, M. *J. Am. Chem. Soc.* **2008**, *130* (47), 15762.
(59) Koumura, N.; Geertsema, E. M.; Meetsma, A.; Feringa, B. L. *J. Am. Chem. Soc.* **2000**, *122* (48), 12005.
(60) Bringmann, G.; Gulder, T.; Gulder, T. A. M.; Breuning, M. *Chem. Rev.* **2011**, *111* (2), 563.
(61) Almenningen, A.; Bastiansen, O.; Fernholt, L.; Cyvin, B. N.; Cyvin, S. J.; Samdal, S. *J. Mol. Struct.* **1985**, *128* (1–3), 59.
(62) Cnossen, A.; Kistemaker, J. C. M.; Kojima, T.; Feringa, B. L. *J. Org. Chem.* **2014**, *79* (3), 927.
(63) Barder, T. E.; Walker, S. D.; Martinelli, J. R.; Buchwald, S. L. *J. Am. Chem. Soc.* **2005**, *127* (13), 4685.
(64) Vicario, J.; Meetsma, A.; Feringa, B. L. *Chem. Commun.* **2005**, *47*, 5910.
(65) $\Delta^{\ddagger}G_{exp}$ within the measured temperature range was used for comparison with $\Delta^{\ddagger}G_{calc}$ to eliminate the error associated with exptrapolation of the data to room temperature.